Justin Chappell
Department of Mechanical Engineering,
University of Utah,
50 S. Central Campus Drive,
MEB 2110,
Salt Lake City, UT 84112-9208

Phil Ligrani[1]
Donald Schultz Professor of Turbomachinery
University of Oxford,
17 Foundry House,
Walton Well Road,
Oxford OX2 6AQ, England
e-mail: p_ligrani@msn.com

Sri Sreekanth
Principal Analyst
Pratt and Whitney Canada,
1801 Courtney Park Drive East,
Mississauga, ON L5A 3S8, Canada
e-mail: sri.sreekanth@pwc.ca

Terry Lucas
Chief, Turbine Cooling and Static Structures
e-mail: terrance.lucas@pwc.ca

Edward Vlasic
Principal Aerodynamicist
e-mail: edward.vlasic@pwc.ca

Pratt and Whitney Canada,
1000 Marie-victorin,
Longueuil, QC, J4G 1A1, Canada

Aerodynamic Performance of Suction-Side Gill Region Film Cooling

The performance of suction-side gill region film cooling is investigated using the University of Utah transonic wind tunnel and a simulated turbine vane in a two-dimensional cascade. The effects of film cooling hole orientation, shape, and number of rows, and their resulting effects on the aerodynamic losses, are considered for four different hole configurations: round axial (RA), shaped axial (SA), round radial (RR), and round compound (RC). The mainstream Reynolds number based on axial chord is 500,000, exit Mach number is 0.35, and the tests are conducted using the first row of holes, or both rows of holes at blowing ratios of 0.6 and 1.2. Carbon dioxide is used as the injectant to achieve density ratios of 1.77–1.99 similar to values present in operating gas turbine engines. Presented are the local distributions of total pressure loss coefficient, local normalized exit Mach number, and local normalized exit kinetic energy. Integrated aerodynamic losses (IAL) increase anywhere from 4% to 45% compared with a smooth blade with no film injection. The performance of each hole type depends on the airfoil configuration, film cooling configuration, mainstream flow Mach number, number of rows of holes, density ratio, and blowing ratio, but the general trend is an increase in IAL as either the blowing ratio or the number of rows of holes increase. In general, the largest total pressure loss coefficient C_p magnitudes and the largest IAL are generally present at any particular wake location for the RR or SA configurations, regardless of the film cooling blowing ratio and number of holes. The SA holes also generally produce the highest local peak C_p magnitudes. IAL magnitudes are generally lowest with the RA hole configuration. A one-dimensional mixing loss correlation for normalized IAL values is also presented, which matches most of the both rows data for RA, SA, RR, and RC hole configurations. The equation also provides good representation of the RA, RC, and RR first row data sets. [DOI: 10.1115/1.3151603]

1 Introduction

Film cooling is employed to maintain gas turbine hot-section components with acceptable temperatures and temperature gradients in order to increase engine performance by allowing operation at higher gas inlet temperature with increased component life. Acceptable temperature levels are a vital characteristic because they lead to less susceptibility high-temperature oxidation, creep, corrosion, and thermomechanical fatigue. Such benefits from film cooling are often offset by the aerodynamic losses they incur. The present paper considers such aerodynamic performance for four different film cooling configurations located on the gill region, suction surface of a turbine vane.

Numerous recent investigations consider various aspects of turbine blade and vane losses, such as the effects of turbulence intensity [1], surface roughness [1], blade row interactions [2], and blade geometry [3]. In an investigation performed by Day et al. [4], which considers the effects of film cooling, a cascade is employed, which operates at conditions similar to those which exist in gas turbine engines. The authors show that utilizing cylindrical holes increases aerodynamic losses by 6.7%, and that utilizing fan-shaped holes increases losses to 15% compared with a no injection condition. They also show that film cooling at the leading edge and early pressure surface region can actually increase aerodynamic efficiency, most likely because of shock/boundary layer interactions. Ito et al. [5] show that losses in incompressible flow can either increase or decrease due to film injection from a single row of holes placed either on the suction or pressure surface. Hong et al. [6] examine the effects of film cooling from a single row of holes located either on the suction surface, pressure surface, or leading edge. The results indicate that the suction surface film cooling has the biggest influence on aerodynamic losses and that pressure surface film cooling has the smallest influence on losses.

Haller and Camus [7] present losses due to film cooling for five separate cooling hole locations on a transonic airfoil, using carbon dioxide to simulate an operating engine density ratio. Their results show that ejection downstream of the passage throat does not necessarily give greater losses than injection upstream of the throat. Kollen and Koschel [8] also utilize carbon dioxide for the film on a transonic airfoil. From this study, losses increase with blowing ratio for film cooling from the leading edge and decrease with blowing ratio when the film cooling is located on the suction surface, except when the blowing ratio is very small.

Of the investigations which examine the effects of augmented freestream turbulence levels, Gregory-Smith and Cleak [9] show that the mean flow field is not affected significantly by inlet turbulence intensity levels as high as 5%. Giel et al. [10] employ an active blowing grid of square bars to produce a turbulent intensity and length scale of 10% and 22 mm, respectively, at the entrance of a transonic cascade. Heat transfer results are given along a turbine airfoil, which show the effects of strong secondary flows, laminar-to-turbulent transition, and variations near the stagnation line. Boyle et al. [11] provide turbine vane aerodynamic data at

[1]Corresponding author.

Contributed by the International Gas Turbine Institute of ASME for publication in the JOURNAL OF TURBOMACHINERY. Manuscript received February 12, 2009; final manuscript received February 26, 2009; published online April 7, 2010. Review conducted by David Wisler. Paper presented at the ASME Turbo Expo 2008: Land, Sea, and Air (GT2008), Berlin, Germany, June 9–13, 2008.

 Copyright © 2010 by ASME

Downloaded 28 May 2010 to 128.113.26.88. Redistribution subject to ASME license or copyright; see http://www.asme.org/terms/Terms_Use.cfm

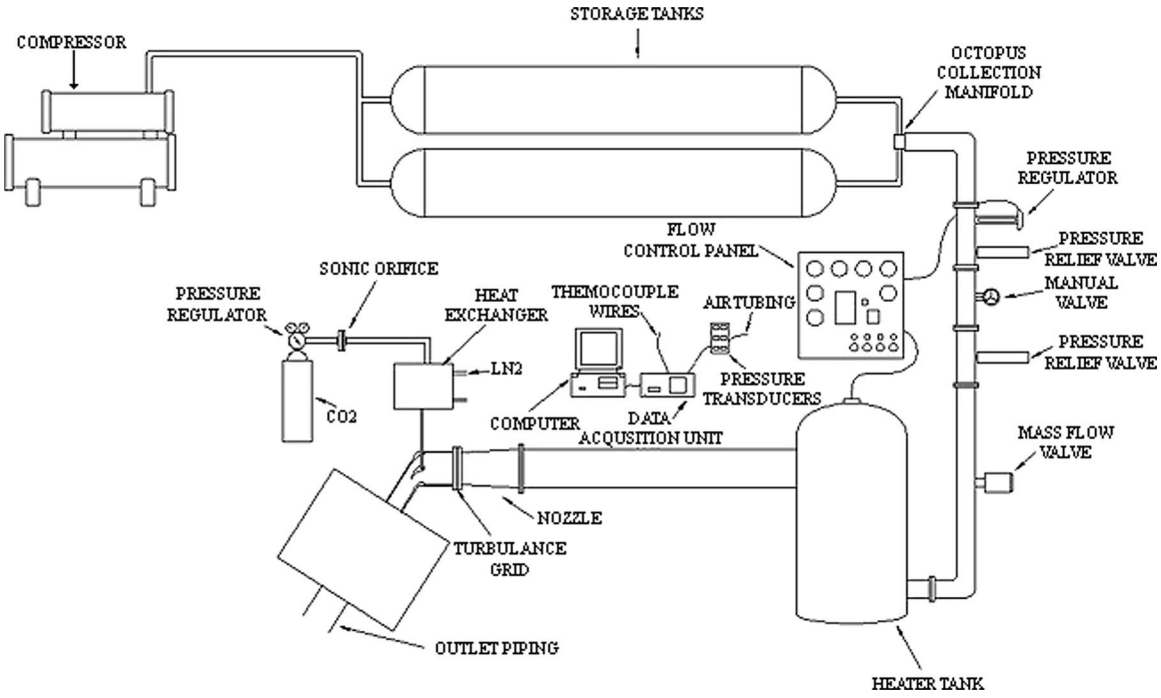

Fig. 1 University of Utah TWT

low Reynolds numbers made at midspan locations downstream of a linear cascade with inlet turbulence intensity levels as high as 10%. In a study of aerodynamic losses downstream of subsonic turbine airfoil with no film cooling, Ames and Plesniak [12] demonstrate important connections between wake growth and the level of freestream turbulence. Jouini et al. [13] present detailed measurements of midspan aerodynamics performance characteristics of a transonic turbine cascade at off-design conditions. Radomsky and Thole [14] present measurements of time-averaged velocity components and Reynolds stresses along a turbine stator vane at elevated freestream turbulence levels. Boyle et al. [15] provide aerodynamic data for a linear turbine vane cascade, including surface pressure distributions and aerodynamic losses for different Reynolds numbers, Mach numbers, and levels of inlet turbulence.

Investigations by Zhang and co-workers [16,17] employ symmetric airfoils with no camber and without significant flow turning. Of these, Zhang et al. [16] investigate the effects of surface roughness and turbulence intensity on the aerodynamic losses produced by the suction surface of a symmetric turbine airfoil. Their results show that the effects of different inlet turbulence intensity levels are generally relatively small. Zhang and Ligrani [17] investigate the effects of surface roughness, freestream Mach number, and turbulence intensity on the aerodynamic performance of turbine airfoils. Their data show that increasing freestream Mach number produce larger magnitudes of nondimensional total pressure loss coefficients. Magnitudes of integrated aerodynamic losses (*IAL*) change by a much larger amount as either the freestream Mach number or turbulence intensity are altered, when the airfoil is roughened (compared with smooth airfoil results).

Of the investigations which examine the effects of Mach number, Christopher et al. [18] show that total pressure losses for a high pressure turbine vane increase approximately with the square of the exit Mach number as a result of a decrease in boundary layer thickness. Coton et al. [19] investigate the effects of Reynolds number and Mach number on the profile losses of a conventional low-pressure turbine rotor cascade and report that the exit Mach number affects the losses through a modification of the pressure gradient imposed on the boundary layer. Their investigations indicate that loss levels are fairly constant with the change of Mach number and are not sensitive to freestream turbulence level.

The present study is focused on the investigation of the effects of film cooling hole shape, orientation, blowing ratio, as well as the number of rows of holes, and their resulting effect on the aerodynamic losses. Also included are the discharge coefficients for the different hole configurations. The film cooling holes are located on the suction-side gill region of a simulated cambered turbine blade. Four different hole configurations are tested at two different blowing ratios, utilizing either a single or two rows of film cooling holes. Carbon dioxide is used as the injectant to achieve a density ratio of 1.9–2.0 similar to values present in operating gas turbine engines. A mesh grid is used to augment the magnitudes of longitudinal turbulence intensity at the inlet of the test section. As such, the present data provide useful information to designers of turbomachinery components and to individuals developing models for computational fluid dynamics (CFD) predictions. Corresponding film cooling effectiveness and heat transfer coefficient data for the same experimental configurations are given in a companion paper [20].

2 Experimental Apparatus and Procedures

2.1 Transonic Wind Tunnel. The University of Utah transonic wind tunnel (TWT) is used for the study and is shown schematically in Fig. 1. The TWT blow-down type facility consists of two main parts: (i) compressor and storage tanks and (ii) wind tunnel. The wind tunnel consists of five major subsections: (i) flow rate and pressure level management apparatus, (ii) plenum tank, (iii) inlet ducting and test section, (iv) plenum, exit ducting, and ejector, and (v) control panel. Detailed descriptions are provided by Ligrani and co-workers [17,21,22].

A Gardner Denver Co. model RL-1155-CB compressor is used to pressurize the array of eight tanks whose total capacity volume is 11.9 m^3. A VanAir VAS93039 model D16-5 deliquescent desiccant dryer, a Pall Corp. 5EHG-4882-207 oil filter, and two Permanent Filter Corp. No. 13846 particulate filters are located just downstream of the compressor to remove particulates and moisture from the air. A Fisher pressure regulator with a 6X4 EWT

Downloaded 28 May 2010 to 128.113.26.88. Redistribution subject to ASME license or copyright; see http://www.asme.org/terms/Terms_Use.cfm

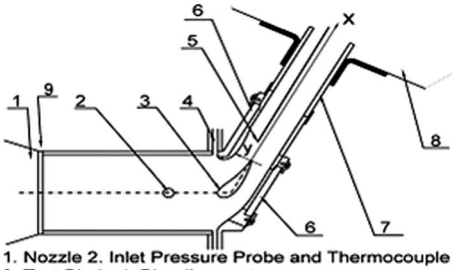

Fig. 2 Schematic of the test section

design sliding gate valve, a Fisher type 667 diaphragm actuator, a 3582 series valve positioner, and a Powers 535 1/4 DIN process controller are used to regulate the pressure in the test section as the storage tanks discharge. A plenum tank, a 30.48 cm inner diameter pipe, a circular-to-square transition duct, a nozzle, and the test section then follow. Relative humidity at the test section inlet is typically 20–30%. The test section is connected to a large $92.71 \times 91.44 \times 91.44$ cm^3 plenum with a square plastic flange at its outlet. The plenum diffuses high speed air from the test section exit into a reservoir of low velocity air. This plenum is then connected to two ducts, which are subsequently connected to the atmosphere.

2.2 Test Section and Test Vane. The present test section is designed to match Reynolds numbers, Mach numbers, pressure gradients, passage mass flow rates, boundary layer development, streamline curvature, airfoil camber, and physical dimensions of turbine vanes in operating aeroengines and in gas turbines used for utility power generation. A schematic of the test section with the cambered vane is shown in Fig. 2. The inlet of the test section is 12.70×12.70 cm^2. The side and bottom walls of the test section are made of steel, and the top wall is made up of acrylic. As shown in Fig. 2, two zinc-selenide windows can be placed on both of the sidewalls, so that the entire airfoil surface is accessible to optical, surface temperature measurement schemes such as infrared thermography. In the present study, a zinc-selenide window is used only on the bottom pressure-surface contour. Of course, no significant radial pressure gradient is present with the arrangement shown in Fig. 2.

Appropriate cascade flow conditions are maintained, in part, by a pair of adjustable bleed ducts, which are located on the two sidewalls, as shown in Fig. 2. The flow rate of each bleed duct is regulated using an adjustable ball valve. Following these, the test section walls have the same pressure-side (PS) and suction-side (SS) contours as the test vane. The exit area and exit flow direction from the cascade test section can be altered by changing the angles of the two exit tailboards, which are also shown in Fig. 2. Thus, (i) changing the total pressure at the test section inlet using the pressure regulator/sliding gate valve arrangement, (ii) changing the angular positions of the two tailboards, and (iii) adjusting the ball valves of the bleeding system are employed to alter the Mach number distribution along the vane in the test section, for a particular vane and test section configuration. By adjusting these items, appropriate Mach number distributions along the test vane are obtained.

Experimental film cooling configurations and conditions employed in the present study are tabulated in Table 1. Table 2 gives geometric parameters of the test vane. The coordinates of this test vane profile were provided by personnel at Pratt and Whitney Canada Corporation, along with the flow conditions present in the associated operating environment.

Table 1 Film cooling experimental conditions

Hole configuration	Blowing ratio	Density ratio
RA first row	0.6	1.77
RA first row	1.2	1.78
RA both rows	0.6	1.82
RA both rows	1.2	1.87
RC first row	0.6	1.82
RC first row	1.2	1.91
RC both rows	0.6	1.94
RC both rows	1.2	1.99
RR first row	0.6	1.79
RR first row	1.2	1.84
RR both rows	0.6	1.86
RR both rows	1.2	1.99
SA first row	0.6	1.85
SA first row	1.2	1.93
SA both rows	0.6	1.91
SA both rows	1.2	1.94

2.3 Film Cooling Hole Configurations. The four different hole configurations which are investigated are shown in Fig. 3: round axial (RA), shaped axial (SA), round radial (RR), and round compound (RC). For each configuration, either the first upstream row of holes only is employed, or two rows of holes are employed. The holes located in each row are staggered with respect to each other. Arrangements with large compound angles are considered because lower manufacturing costs are generally associated with this type of hole geometry. As shown in Fig. 4, the hole exits for all four arrangements are located at 15% and 25% of the axial chord. In addition, the holes in each row have the same spanwise hole diameter spacing of $6d$. The row of holes marked A-A in Fig. 3 contains 13 film cooling holes, and the row of holes marked by B-B in Fig. 3 contains 14 film cooling holes. Note that the RR and RC configurations are unique because of the large compound angles which are employed.

2.4 Secondary Film Coolant Injection System. Carbon dioxide is used as the injectant to achieve density ratios similar to those experienced in operating gas turbine engines, $\rho_c/\rho_\infty = 1.77-1.99$. With the present secondary injection system arrangement, regulated carbon dioxide leaves its tank and first goes through a sonic orifice, which is used in conjunction with pressure and temperature measurements to determine the injectant mass flow rate. After leaving the sonic orifice, the injectant enters a TV-050 heat exchanger (also shown in Fig. 1), which uses liquid nitrogen as a coolant. As the injectant is cooled, it is passed through bypass valves until the mainstream air is started, to prevent any advance cooling of the vane. Just prior to the mainstream blow down, valves are arranged so that the injectant flows through the vane and out of the film cooling holes. To approximate a plenum condition, the injectant enters the injectant passage from both the top and bottom of the vane. Because carbon dioxide instead of air is employed, the ratio of specific heats only approximates values that exist in operating engines.

2.5 Pressure and Temperature Measurements. As tests are conducted, Validyne model DP15-46 pressure transducers (with

Table 2 Test vane geometric parameters

Parameter	Unit	Value
True chord (C)	cm	7.27
Axial chord (Cx)	cm	4.85
Pitch (p)	cm	6.35
Span	cm	12.7
Flow turning angle	deg	62.75

Downloaded 28 May 2010 to 128.113.26.88. Redistribution subject to ASME license or copyright; see http://www.asme.org/terms/Terms_Use.cfm

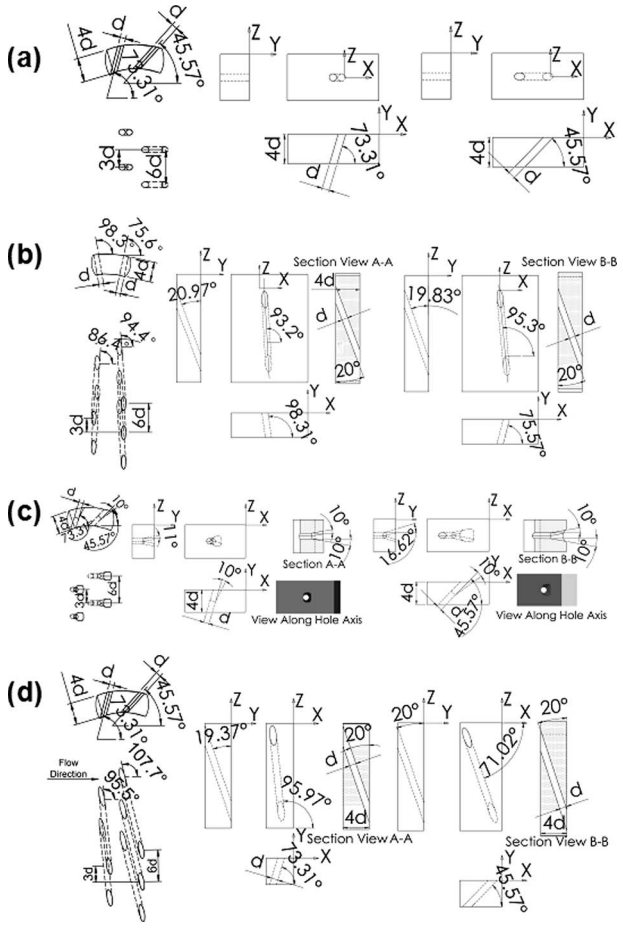

Fig. 3 Film cooling hole configurations: (*a*) RA, (*b*) RR, (*c*) SA, and (*d*) RC

diaphragms rated at either 34.5 kPa or 344.7 kPa) and calibrated copper-constantan thermocouples are used to sense pressures and temperatures at different locations throughout the facility. Signals from the pressure transducers are processed by Celesco model CD10D carrier demodulators. All pressure transducer measurement circuits are calibrated using a Wallace and Tiernan FA145 bourdon tube pressure gage as a standard. A United Sensor PLC-8-KL pitot-static probe with an attached, calibrated Watlow standard type-K copper-constantan thermocouple, and a four-hole conical-tipped pressure probe also with a similar Watlow thermocouple are used to sense total pressure, static pressure, and recovery temperature at the inlet and exit of the test section, respectively, during each blow down. Mach numbers, sonic velocities, total temperatures, and static temperatures are determined from these data. The four-hole probe has a tip, which is 1.27 mm in diameter, and a stem, which is 3.18 mm in diameter. Each port has a diameter of 0.25 mm. The overall response time of the pressure measuring system is about 0.2 s. The conical probe is aligned using two yaw ports placed on either side of the probe. The probe is located downstream of the vane. The position in the streamwise direction is adjustable. As a blow down is underway, it is traversed across a full pitch using a two-axis traversing sled with two Superior Electric M092-FF-206 synchronous stepper motors, connected to a Superior Electric model SS2000I programmable motion controller and a Superior Electric model SS2000D6 driver. Commands for the operation of the motion controller are provided by LABVIEW 7.0 software and pass though a serial port after they originate in a Dell Precision 530 PC workstation. Each profile is measured through the wake from minus y/Cx locations to positive y/Cx locations, and then repeated as the probe is traversed in the opposite direction. The resulting data are subsequently averaged at each wake measurement location. Such wake profiles are measured at three different spanwise locations downstream the blade trailing edge to determine variations with spanwise location.

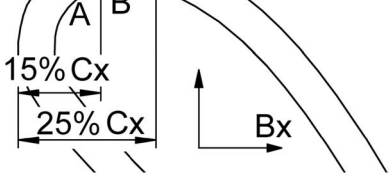

Fig. 4 Film cooling hole locations

Voltages from the carrier demodulators and thermocouples are read sequentially using Hewlett-Packard HP44222T and HP44222A relay multiplexer card assemblies, installed in a Hewlett-Packard HP3497A low-speed data acquisition/control unit. This system provides thermocouple compensation electronically such that voltages for type-T thermocouples are given relative to 0°C. The voltage outputs from this unit are acquired by the Dell Precision PC workstation through its USB port, using LABVIEW 7.0 software and a GPIB-USB-B adaptor made by National Instruments.

2.6 Mainstream Flow Turbulence Level. A fine mesh grid arrangement is used at the inlet of the test section to augment the magnitude of mainstream turbulence intensity [23]. The fine mesh grid consists of an array of four square rods arranged horizontally and four square rods arranged vertically. Each rod is spaced 25.4 mm from adjacent rods and is 5 mm on each side. The open area amounts to 48% of the inlet area. The installation position for the fine mesh grid is at the exit of the nozzle shown in Fig. 2.

2.7 Longitudinal Turbulence Intensity Measurements. A single horizontal-type platinum-plated tungsten hot-wire sensor, with a diameter of 12.7 μm and a length of 2.54 mm, is employed to measure the time-varying longitudinal component of velocity at the inlet of the test section. The time-averaged longitudinal velocity and the longitudinal turbulence intensity are then determined from these measurements. The measurement location is one axial chord length upstream of the vane leading edge. The hot-wire probe is driven by a Disa 55M10 constant-temperature hot-wire anemometer bridge with an overheat ratio of 1.6. The analog signal from this bridge is then processed using a Dantec 56N20 signal conditioner with a low-pass anti-aliasing filter set to 100 kHz. The time-varying output voltage signal is then sampled at a 200 kHz rate using a Datel PCI441D I/O board installed in the Dell Precision 530 PC workstation. During each measurement, 2×10^6 voltage values are sampled over a time period of 10 s. Data are acquired using LABVIEW 7.0 software and then processed further using MATLAB 6.1 software. The entire measurement system, including the hot-wire sensor, is calibrated in the freestream of the TWT. A Kiel type pressure probe, wall static taps, and a copper-constantan thermocouple are used to measure and determine the total pressure, static pressure, recovery temperature, and velocity at the inlet of the test section as the calibration is conducted.

2.8 Experimental Uncertainties. Uncertainty estimates are based on 95% confidence levels and determined using procedures described by Kline and McClintock [24] and by Moffat [25]. Mach number uncertainty is 0.002. Uncertainty of temperatures is 0.15°C. Pressure uncertainty is 0.25 kPa. Uncertainties of C_p, M_e/M_e, and KE are 0.0013 (0.07), 0.0023 (0.96), and 0.03 (0.90), respectively, where typical nominal values of these quantities are

Downloaded 28 May 2010 to 128.113.26.88. Redistribution subject to ASME license or copyright; see http://www.asme.org/terms/Terms_Use.cfm

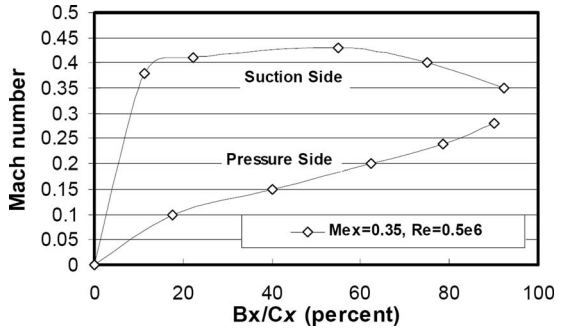

Fig. 5 Vane Mach number distribution

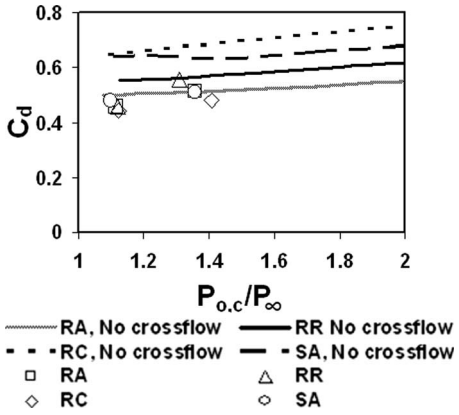

Fig. 6 Vane film cooling hole discharge coefficients for first row of holes only

given in parentheses. *IAL* uncertainty is 0.04 N/cm (0.800 N/cm). Magnitudes of *IAL*, determined from replicate runs, are always within *IAL* uncertainty ranges.

3 Experimental Results

3.1 Test Section Flow Characteristics and Mach Number Distributions. During each blow down test, the total pressure, Reynolds number, and turbulence level at the test section inlet are maintained in a continuous and steady fashion for up to 45 s long time intervals, as detailed by Jackson et al. [21]. Such characteristics are not only a result of TWT design but also the excellent performance of the TWT mainstream air pressure regulator and its controller. During each test, the inlet total pressure at the inlet of the test section (one axial chord length upstream of the vane leading edge) is maintained constant at 94 kPa. This corresponds to an exit freestream Mach number of 0.35 and an exit Reynolds number based on axial chord of 0.5×10^6, as measured 0.25 axial chord lengths downstream the airfoil trailing edge.

The magnitudes of the inlet mainstream longitudinal turbulence intensity and length scale for the present experimental conditions are 5.7% and 2.2 cm, respectively. As such, these values are approximately representative of the associated combustor exit flow. Here, turbulence intensity is defined as the ratio of the root mean square of the longitudinal fluctuation velocity component divided by the local streamwise mean component of velocity. The autocorrelation function is integrated with respect to the time lag to obtain the longitudinal integral time scale, which is then multiplied by the mean velocity to get the longitudinal integral length scale, which is a representative of the largest eddies in the turbulent flow field.

Inlet uniformity measurements are conducted at five different pitchwise locations at the inlet of the test section. With no turbulence grid employed, the total pressure and static pressure show excellent spatial uniformity at this location, varying by less than 0.5% of mean values. With the fine mesh grid, the total pressure and static pressure generally vary less than 0.6% of mean values. Note that the fine mesh grid is installed approximately 5.2 axial chord lengths away from the leading edge of the vane to maintain an acceptable level of uniformity in the flow as it approaches the vane.

Figure 5 shows the Mach number distributions along the turbine vane pressure side and along the vane suction side for the present operating conditions. The data shown in this figure are based on measurements of total pressure at the test section inlet and vane midspan static pressures. Compressible flow analysis in the form of isentropic relations is used to calculate Mach number distributions around the vane. These are measured using an airfoil that is constructed especially for this task. The vane has five pressure taps on the pressure side and five pressure taps on the suction side, as well as one pressure tap located on the leading edge at the vane midspan. As shown in Fig. 5, the Mach number distribution employed in this study is subsonic on the vane suction and pressure sides, with an adverse pressure gradient on the suction side of the vane when $Bx/Cx>0.60$. As such, the present Mach number distribution is in excellent agreement with data for gas turbine vanes from industry [23].

3.2 Discharge Coefficients. Discharge coefficients are determined using the equation given by

$$C_D = \dot{m}_{\text{act}}/\dot{m}_{\text{ideal}} \tag{1}$$

where the ideal mass flow rate is obtained using

$$\dot{m}_{\text{ideal}} = AP_{o,c}M_c\sqrt{\frac{k_c}{RT_{o,c}}}\left[1+\frac{(k_c-1)}{2}M_c^2\right]^{-(k_c+1)/2(k_c-1)} \tag{2}$$

Here, A is the total cross-sectional area of the holes at their round inlets and M_c is the isentropic Mach number of the injectant at the exits of the film cooling holes. This Mach number is determined using an isentropic relation based on the ratio of the stagnation pressure in the injection plenum $P_{o,c}$ and the static pressure at the exits of the film cooling holes P_∞.

Results for the discharge coefficients are shown in Figs. 6 and 7. Results are presented at various injectant to freestream pressure ratios, both with and without a freestream cross-flow. For each film cooling configuration, results are given for two arrangements: first row only (Fig. 6) and both rows of film cooling holes (Fig. 7). The discharge coefficient performance of the different hole configurations depends on whether the first row or both rows of film cooling holes are used, as well as the pressure ratio and flow condition. In general, discharge coefficient values with no cross-flow are higher than values with cross-flow when compared at a particular value of the $P_{o,c}/P_\infty$ pressure ratio. The discharge coefficients presented in Figs. 6 and 7 generally increase with pressure ratio for each film cooling configuration. In addition, dis-

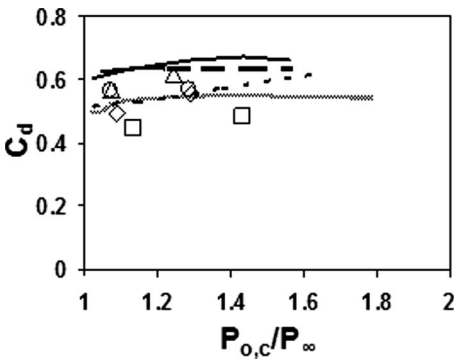

Fig. 7 Vane film cooling hole discharge coefficients for both rows of holes. Symbols and lines are defined in Fig. 6.

Downloaded 28 May 2010 to 128.113.26.88. Redistribution subject to ASME license or copyright; see http://www.asme.org/terms/Terms_Use.cfm

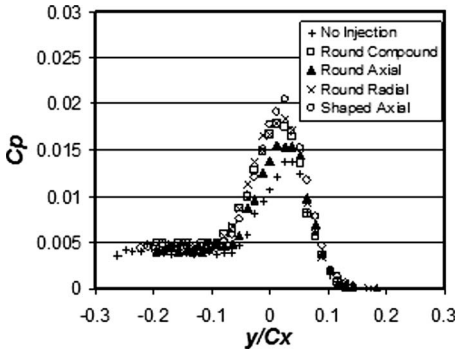

Fig. 8 Local pressure loss coefficient profiles for injection from the first row of holes only with a blowing ratio of 0.6

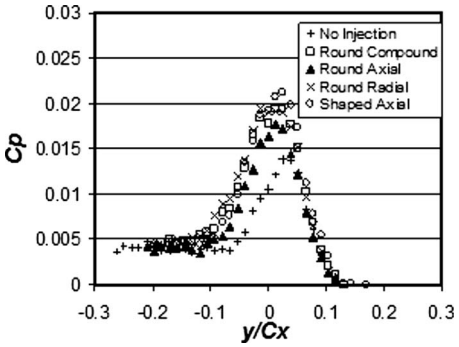

Fig. 11 Local pressure loss coefficient profiles for injection from both rows of holes with a blowing ratio of 1.2

charge coefficients are generally higher for the both row configuration than for the first row configuration, except for the round axial hole arrangement. Overall, the total variation in discharge coefficients varies approximately from 0.44 to 0.77.

3.3 Local Aerodynamic Losses. Local aerodynamic loss profiles, in the form of total pressure loss coefficients C_p and measured 0.25 axial chord lengths downstream of the vane, are presented in Figs. 8–11. Figure 8 presents data for the first row of holes only with a blowing ratio of 0.6, Fig. 9 presents data for the first row of holes only with a blowing ratio of 1.2, Fig. 10 presents data for both rows of holes only with a blowing ratio of 0.6, and Fig. 11 presents data for both rows of holes only with a blowing ratio of 1.2. Recall that such wake profiles are measured at three different spanwise locations downstream the blade trailing edge to determine variations with spanwise location. In general, no spanwise variations are present for the RA and SA hole configurations; however, some spanwise variations are sometimes present for the RC and RR arrangements. For the former case, all three of the spanwise profiles are averaged to obtain the results given in Figs. 8–15, and for the latter, two of the three profiles are averaged to obtain the results given in Figs. 8–15.

Aerodynamic losses from film cooling are a result of several mechanisms. These include mixing losses due to differences between coolant and mainstream/boundary layer stagnation pressures and/or stagnation temperatures. When these are present, film

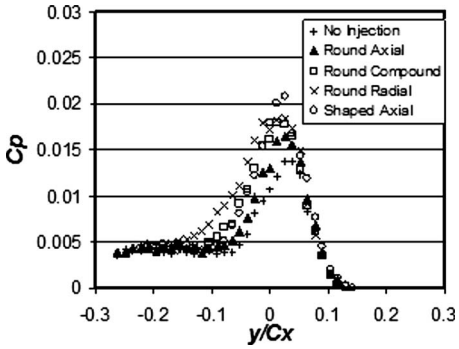

Fig. 9 Local pressure loss coefficient profiles for injection from the first row of holes only with a blowing ratio of 1.2

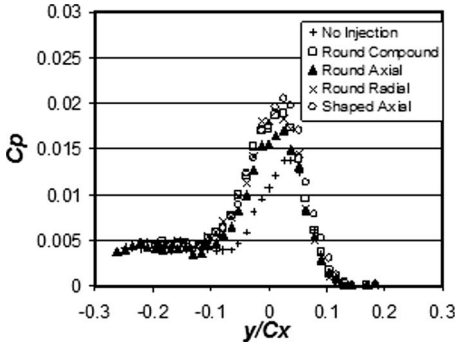

Fig. 10 Local pressure loss coefficient profiles for injection from both rows of holes with a blowing ratio of 0.6

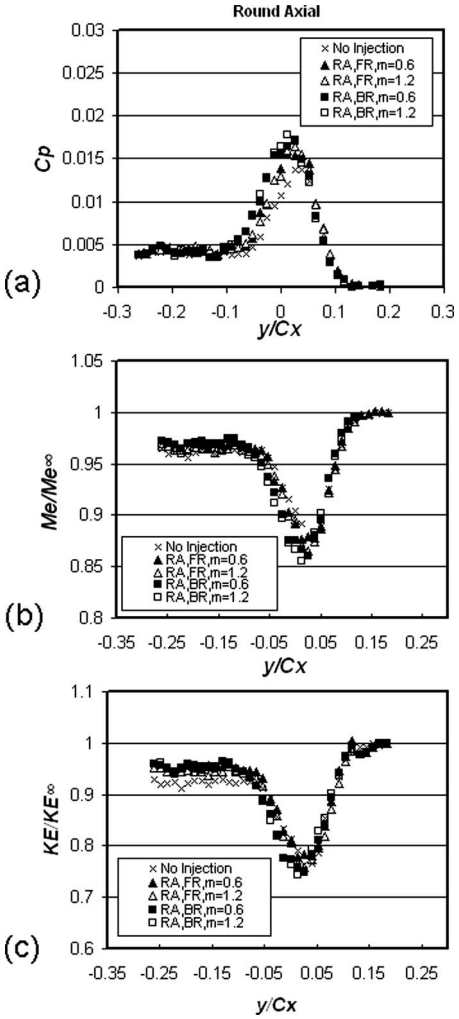

Fig. 12 Aerodynamic loss profiles for the RA holes: (*a*) pressure loss coefficients, (*b*) normalized Mach numbers, and (*c*) normalized kinetic energies

Downloaded 28 May 2010 to 128.113.26.88. Redistribution subject to ASME license or copyright; see http://www.asme.org/terms/Terms_Use.cfm

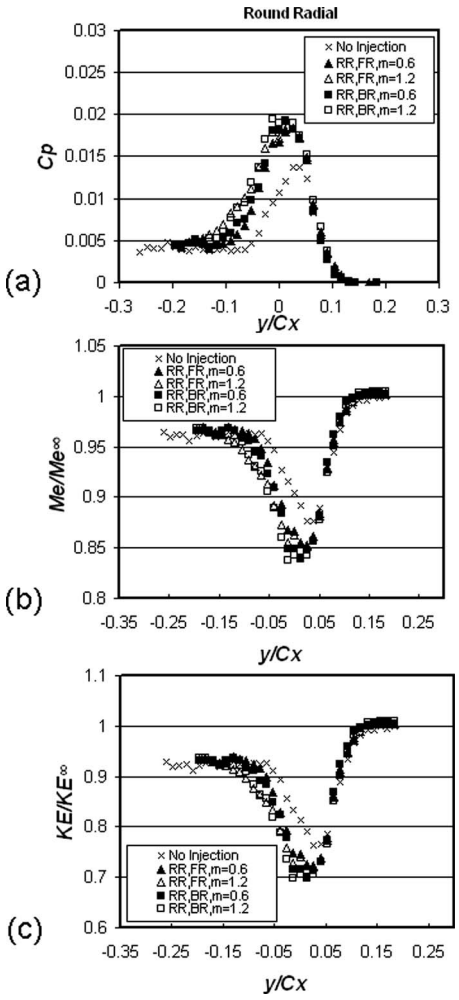

Fig. 13 Aerodynamic loss profiles for the RR holes: (*a*) pressure loss coefficients, (*b*) normalized Mach numbers, and (*c*) normalized kinetic energies

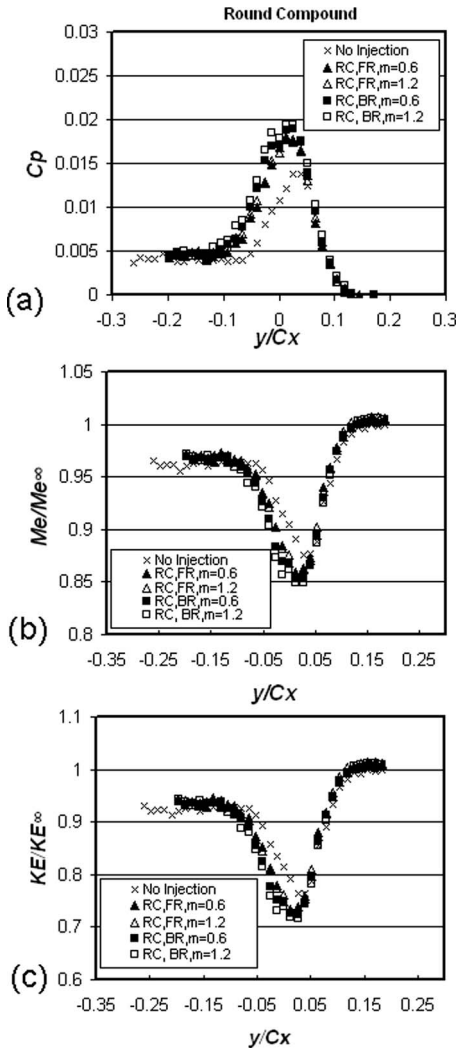

Fig. 14 Aerodynamic loss profiles for the RC holes: (*a*) pressure loss coefficients, (*b*) normalized Mach numbers, and (*c*) normalized kinetic energies

cooling often increases magnitudes of Reynolds stress tensor components in the boundary layers. Such mixing is thus connected to alterations of shear stress distributions resulting from differences in velocity magnitudes and/or flow direction between the film coolant and the mainstream. As such, film cooling also often results in changes to kinetic energy distributions within blade and vane boundary layers.

Because of the alterations to airfoil boundary layer development, which result from film cooling, aerodynamic losses at airfoil trailing edges and overall airfoil losses are present, in part, because of changes to local boundary layer thickness. Note that if the jet exiting from film cooling holes has a relatively high streamwise momentum, the resulting downstream boundary layer may be thinned, which could result in more severe separation at the trailing edge. This would increase aerodynamic losses. Opposite effects may be observed if the downstream boundary layer is thickened by a coolant jet with low streamwise momentum content. However, in this case, even though the separation may be less severe, downstream aerodynamic losses increase because of increases in trailing edge boundary layer thickness. According to Bammert and Sandstede [26], the boundary layer on the suction side is generally much thicker than on the pressure side, and wake profile losses are caused more by suction-side events than by events on the pressure side, by a factor of 2.5–3.5 times.

Figures 8–11 generally show that the introduction of film cooling increases local stagnation pressure losses. This is evidenced by comparisons of the film cooling data with the no injection data. In general, most of these losses occur over $-0.1 < y/Cx < 0.05$ because the film cooling holes are located on the suction side of the vane. The largest C_p magnitudes and the largest aerodynamic losses are generally present at any particular y/Cx value within this range for the RR or SA configurations, regardless of the film cooling blowing ratio and number of holes. The SA holes also generally produce the highest peak C_p magnitudes. This is likely due, in part, to diffusion influences of these hole shapes. The smallest losses are generally present for the RA configuration. In many cases, the introduction of film cooling also results in additional thickening of suction-side wakes, compared with the no injection situation. Note that all of the no injection data, which are presented in Figs. 8–11, are in excellent agreement with the results of Zhang et al. [23].

3.4 Local Aerodynamic Loss, Mach Number, and Kinetic Energy Distributions. Figures 12–15 present the profiles of total pressure loss coefficient C_P, normalized exit Mach number $M_e/M_{e\infty}$, and normalized exit kinetic energy KE/KE_∞, where exit refers to values measured 0.25 chord lengths downstream of the vane trailing edge. Results for RA holes are given in Figs. 12(*a*)–12(*c*), results for RR holes are given in Figs. 13(*a*)–13(*c*), results for RC holes are given in Figs. 14(*a*)–14(*c*), and results for SA holes are given in Figs. 15(*a*)–15(*c*). As mentioned, film in-

Downloaded 28 May 2010 to 128.113.26.88. Redistribution subject to ASME license or copyright; see http://www.asme.org/terms/Terms_Use.cfm

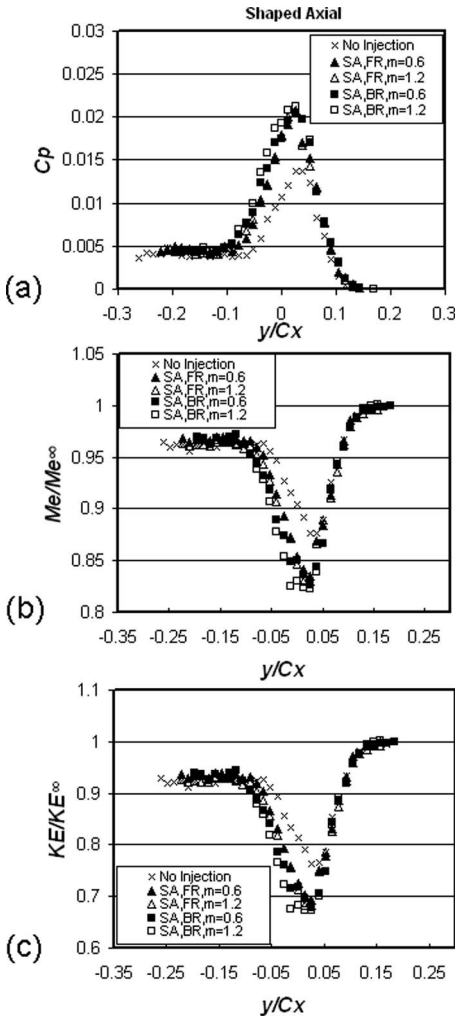

Fig. 15 Aerodynamic loss profiles for the SA holes: (*a*) pressure loss coefficients, (*b*) normalized Mach numbers, and (*c*) normalized kinetic energies

jection test conditions are given in Table 1, where ρ_c/ρ_∞ density ratios range from 1.77 to 1.99. Note that all film cooling parameters in Table 1 are based on hole *inlet* areas, and that the inlet freestream stagnation pressure $P_{oi\infty}$ is approximately 94 kPa. All of the no injection data, which are presented in Figs. 12–15, are in excellent agreement with the results that are presented by Zhang et al. [23]. Here, FR refers to the first row of holes, and BR refers to both rows of holes.

Overall qualitative trends of the data in Figs. 12–15 are similar for the SA, RC, and RA configurations, with somewhat different trends for the RR arrangement. With regard to the first three of these, in general, both the $m=0.6$ and $m=1.2$ *both row data* show greater C_P magnitudes, lower KE/KE_∞ values, and lower $M_e/M_{e\infty}$ values, compared with both sets of the $m=0.6$ and $m=1.2$ *first row data*, when compared at a particular y/Cx value. Because the film cooling holes are located on the suction side of the vane, these variations are most apparent for $-0.1<y/Cx<0.05$. When either the both row or first row data are considered by themselves, the $m=1.2$ data often show slightly higher C_P magnitudes, slightly lower KE/KE_∞ values, and slightly lower $M_e/M_{e\infty}$ values, than the $m=0.6$ data.

In contrast to these trends, the RR data in Fig. 13 show stronger dependence on the blowing ratio m. This is evident because all of the $m=1.2$ C_P data (for first row of holes and both rows of holes) are generally higher than the $m=0.6$ C_P data (for first row of holes and both rows of holes), when compared at a particular y/Cx value. Corresponding normalized kinetic energy and Mach number data for $m=1.2$ are then generally lower than the $m=0.6$ data. In this case, these variations are apparent for $-0.2<y/Cx<0.05$ partially because of additional suction surface wake broadening, which is produced by the RR hole arrangement. Additional scrutiny of these results shows somewhat larger changes (higher C_P, lower KE/KE_∞, and lower $M_e/M_{e\infty}$) for the BR arrangement than for the FR arrangement at particular y/Cx values for a particular magnitude of blowing ratio.

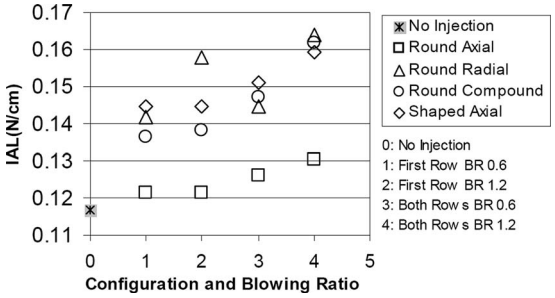

Fig. 16 Dimensional integrated aerodynamic loss values for different hole configurations, number of rows of holes, and blowing ratios

3.5 Integrated Aerodynamic Losses. *IAL* are found by integrating profiles of $(P_{oi}-P_{oe})$ with respect to y in the transverse flow direction across the wake for a single vane spacing, from $-p/2$ to $p/2$. This is equivalent to y/C_x from -0.27 to $+0.27$.

$$IAL=\int_{-p/2}^{p/2}(P_{oi}-P_{oe})dy \tag{3}$$

All *IAL* values are determined from profiles such as the ones presented in Figs. 8–15 measured 0.25 axial chord lengths downstream the turbine vane. Dimensional magnitudes of *IAL* are given in Fig. 16 for the different film configurations investigated. Here, *IAL* values vary from approximately 0.117 N/cm to approximately 0.164 N/cm. From this figure, it is evident that the RA holes produce the lowest *IAL* values, whereas either the RR or SA holes often give the highest *IAL* magnitudes.

Figures 17 and 18 present normalized integrated aerodynamic loss data, after subtracting off the *IAL* value for no film cooling. These data are given as they depend on blowing ratio, and show important variations with film cooling hole configuration and arrangement. In Fig. 18 (which presents both row data), differences between the RR, RC, and SA sets of *IAL* data are quite small, with *IAL* values that are significantly higher than ones produced by the RA configuration (at particular blowing ratio values). In all cases,

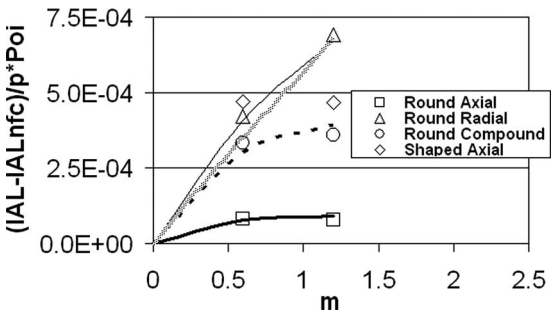

Fig. 17 Normalized integrated aerodynamic loss values for different hole configurations for film injection from the first row of holes only

Downloaded 28 May 2010 to 128.113.26.88. Redistribution subject to ASME license or copyright; see http://www.asme.org/terms/Terms_Use.cfm

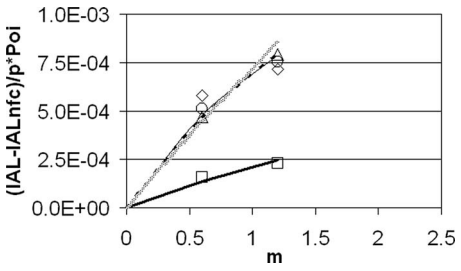

Fig. 18 Normalized integrated aerodynamic loss values for different hole configurations for film injection from both rows of holes. Symbols are defined in Fig. 17.

IAL values increase continuously with blowing ratio. *IAL* values in Figs. 17 and 18 are compared with the one-dimensional mixing loss equation given by

$$(IAL - IAL_{\text{nfc}})/pP_{oi\infty} = C_1[kM_\infty^2/2](\dot{m}_c/\dot{m}_\infty)B \tag{4}$$

where C_1 values are given in Table 3 for the different film cooling arrangement investigated, and

$$B = [1 + T_{oc}/T_{oi\infty} - [2(u_c/u_\infty)\cos\ \theta]] \tag{5}$$

This equation is similar to the one given by Denton [27]. In both cases, M_∞, $\dot{m}_\infty$, and u_∞ are freestream values at the streamwise locations of the film cooling holes. Equations (4) and (5) show good agreement with much of the data in Figs. 17 and 18, including its dependence on blowing ratio m and number of rows of film cooling holes. In particular, the correlation equation matches most of the both row data in Fig. 18. In Fig. 17 for the first row data, the RA, RC, and RR data sets are well aligned with the correlation equations (4) and (5).

The results in Fig. 19 are presented to illustrate the influences of airfoil configuration, film cooling configuration, blowing ratio, and mainstream flow Mach number on normalized integrated aerodynamic losses. Here, the present first row data are compared with the data from Jackson et al. [21], which are measured downstream of an airfoil with a single row of conical diffused holes located on one side. In this figure, the data of Jackson et al. [21] are significantly higher than the present results, when compared at a particular blowing ratio. This is believed to be mostly a consequence of the transonic flow conditions and the symmetric airfoil arrangement with suction surface contours on both sides, which are employed by Jackson et al. [21].

Table 3 C_1 values

Hole configuration	First row	Both rows
Round axial	0.29	0.70
Round compound	4.78	2.71
Round radial	3.93	2.70
Shaped axial	2.10	2.40

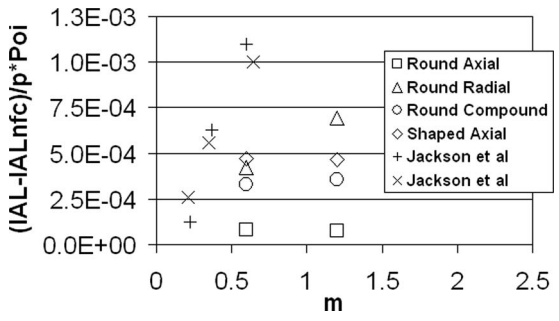

Fig. 19 Normalized integrated aerodynamic loss values for different hole configurations for film injection from the first row of holes only, including comparisons with the data of Jackson et al. [21]

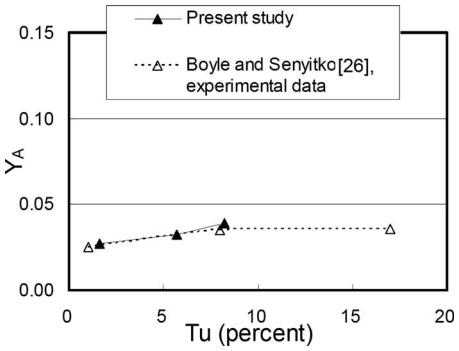

Fig. 20 Comparison of area-averaged loss coefficients with values from Ref. [28]

3.6 Area-Averaged Loss Coefficients. Different loss coefficient definitions are sometimes employed by different research groups. Of these, Boyle and Senyitko [28] employed an area-averaged loss coefficient Y_A in their analysis, which is defined using an equation of the form

$$Y_A = \frac{p_{oi} - p_{oe,A}}{p_{oi} - p_{se,A}} \tag{6}$$

Here, $p_{oe,A}$ and $p_{se,A}$ are the area averaged exit total pressure and static pressure, respectively. These are determined using equations, respectively, given by

$$p_{oe,A} = \int_{-p/2}^{p/2} p_{oe} d(y/p) \tag{7}$$

and

$$p_{se,A} = \int_{-p/2}^{p/2} p_{se} d(y/p) \tag{8}$$

Boyle and Senyitko [28] employed vanes with 5.18 cm axial chord length and 75 deg flow turning angle. Their data are based on measurements made in axial plane located 0.29 axial chord length downstream of their vane trailing edge. Figure 20 shows comparisons of their data with results from the present study, which are measured in normal planes $0.25Cx$ downstream of the vane. These data indicate that higher Y_A losses are generally observed as higher inlet turbulence intensity levels are present. Excellent agreement is shown in Fig. 20 between the results from Ref. [28] and the present study at relatively low exit Mach number. For the present study, $M_{ex}=0.35$ and $\text{Re}=0.5\times10^6$, whereas $M_{ex}=0.3$ and approximately $\text{Re}=0.52\times10^6$ for Ref. [28]. Note that different wake traversing procedures are used in the present study and by Boyle and Senyitko [28]. Whereas profiles from the present study are measured in planes, which are oriented normal to the backflow direction, wake data from their investigation [28] are given for axial planes.

4 Summary and Conclusions

The performance of suction-side gill region film cooling is investigated using the University of Utah transonic wind tunnel and a simulated turbine vane in a two-dimensional cascade. The effects of film cooling hole orientation, shape, and number of rows, and their resulting effects on the aerodynamic losses, are considered for four different hole configurations: RA, SA, RR, and RC. The mainstream Reynolds number based on axial chord is 500,000, exit Mach number is 0.35, and the tests are conducted using the first row of holes, or both rows of holes at blowing ratios

Downloaded 28 May 2010 to 128.113.26.88. Redistribution subject to ASME license or copyright; see http://www.asme.org/terms/Terms_Use.cfm

of 0.6 and 1.2. Carbon dioxide is used as the injectant to achieve density ratios of 1.77 to 1.99 similar to the values present in operating gas turbine engines. Presented are the local distributions of total pressure loss coefficient, local normalized exit Mach number, and local normalized exit kinetic energy, along with *IAL* magnitudes and area-averaged loss coefficients.

IAL increase anywhere from 4% to 45% compared with a smooth blade with no film injection. The performance of each hole type depends on the airfoil configuration, film cooling configuration, mainstream flow Mach number, number of rows of holes, density ratio, and blowing ratio, but the general trend is an increase in *IAL* as either the blowing ratio or the number of rows of holes increases. When both rows of hole *IAL* data are considered, differences between the RR, RC, and SA sets are quite small, with *IAL* values that are significantly higher than the ones produced by the RA configuration (at a particular blowing ratio). Normalized *IAL* values are compared with a one-dimensional mixing loss correlation, which matches most of the both row data for RA, SA, RR, and RC hole configurations. The equation also provides good representation of the RA, RC, and RR first row data sets.

The increased local stagnation pressure losses from film cooling are mostly apparent over $-0.1 < y/Cx < 0.05$ because the film cooling holes are located on the suction side of the vane. Here, the largest C_p magnitudes and the largest aerodynamic losses are generally present at any particular y/Cx value within this range for the RR or SA configurations, regardless of the film cooling blowing ratio and number of holes. The SA holes also generally produce the highest peak C_p magnitudes. *IAL* magnitudes are lowest with the RA hole configuration.

Overall qualitative trends of the total pressure loss, exit Mach number, and kinetic energy data are similar for the SA, RC, and RA configurations, with somewhat different trends for the RR arrangement. With regard to the first three of these, in general, both the $m=0.6$ and $m=1.2$ both row data show greater C_P magnitudes, lower KE/KE_∞ values, and lower $M_e/M_{e\infty}$ values, compared with both sets of the $m=0.6$ and $m=1.2$ first row data, when compared at a particular y/Cx value. In contrast to these trends, the RR data show stronger dependence on the blowing ratio m. This is evident because all of the $m=1.2$ C_P data (for first row of holes and both rows of holes) are generally higher than the $m=0.6$ C_P data (for first row of holes and both rows of holes), when compared at a particular y/Cx value.

Acknowledgment

The authors gratefully acknowledge Pratt and Whitney Canada, who sponsored this research effort. Dr. Qiang Zhang is also acknowledged for his guidance with regard to arrangement and operation of different test apparatus components.

Nomenclature

A = area of film cooling holes
Bx = vane axial chord coordinate
C = true chord length
C_D = discharge coefficient
Cx = vane axial chord length
C_p = local total pressure loss coefficient, $(P_{oi}-P_{oe})/P_{oi}$
k = ratio of specific heats
$\dot{m}_{\text{act}}$ = actual mass flow rate of injectant
$\dot{m}_{\text{ideal}}$ = ideal mass flow rate of injectant
M_c = Mach number of injectant at hole exits
M_e = exit local Mach number
$M_{e,\infty}$ = exit freestream Mach number
KE = normalized local kinetic energy, $(P_{oe}-P_{se})/(P_{oe}-P_{se})_\infty$
m = blowing ratio
$\dot{m}$ = mass flow rate
M = Mach number
p = passage pitch
P_o = stagnation pressure
$P_{o,c}$ = stagnation pressure of injectant in plenum
P_{oe} = exit local stagnation pressure
$P_{oe\infty}$ = exit freestream stagnation pressure
P_{oi} = inlet local stagnation pressure
$P_{oi\infty}$ = inlet freestream stagnation pressure
P_{se} = exit local static pressure
P_{oem} = mass averaged exit stagnation pressure
$p_{oe,A}$ = area averaged exit stagnation pressure
$p_{se,A}$ = area averaged static pressure
T = temperature
Tu = test section inlet longitudinal turbulence intensity level
u = local velocity
x = linear distance downstream of the vane measured from the vane trailing edge
X = film cooling hole streamwise coordinate
y = normal coordinate measured from vane centerline
Y = film cooling hole normal coordinate
Y_A = area-averaged loss coefficient
Z = film cooling hole spanwise coordinate

Greek Symbols

θ = film cooling holes inclination angle
ρ = local density

Subscripts

A = area-averaged
c = injectant or film coolant value at exit planes of film cooling holes
∞ = local freestream value
i = inlet of test section
e = exit of test section
nfc = no film cooling
o = total or stagnation
ideal = ideal isentropic value

References

[1] Zhang, Q., and Ligrani, P., 2006, "Aerodynamic Losses of a Cambered Turbine Vane: Influences of Surface Roughness and Freestream Turbulence Intensity," ASME J. Turbomach., **128**, pp. 536–546.
[2] Pullan, G., 2006, "Secondary Flows and Loss Caused by Blade Row Interaction in a Turbine Stage," ASME J. Turbomach., **128**, pp. 484–491.
[3] Benner, M., Sjolander, S., and Moustapha, S., 2004, "Shock Wave-Film Cooling Interactions in Transonic Flows," ASME J. Turbomach., **126**, pp. 277–287.
[4] Day, C. R. B., Oldfield, M. L. G., and Lock, G. D., 2000, "Aerodynamic Performance of an Annular Cascade of Film Cooled Nozzle Guide Vanes Under Engine Representative Conditions," Exp. Fluids, **29**, pp. 117–129.
[5] Ito, S., Eckert, E. R. G., and Goldstein, R. J., 1980, "Aerodynamic Loss in a Gas Turbine Stage With Film Cooling," ASME J. Eng. Power, **102**, pp. 964–970.
[6] Hong, Y., Fu, C., Cunzhong, G., and Zhongqi, W., 1997, "Investigation of Cooling-Air Injection on the Flow Field Within a Linear Turbine Cascade," ASME Paper No. 97-GT-520.
[7] Haller, B. R., and Camus, J. J., 1984, "Aerodynamic Loss Penalty Produced by Film Cooling Transonic Turbine Blades," ASME J. Eng. Gas Turbines Power, **106**, pp. 198–205.
[8] Kollen, O., and Koschel, W., 1985, "Effect of Film-Cooling on the Aerodynamic Performance of a Turbine Cascade," Paper No. AGARD CP-390.
[9] Gregory-Smith, D. G., and Cleak, J. G. E., 1992, "Secondary Flow Measurements in a Turbine Cascade With High Inlet Turbulence," ASME J. Turbomach., **114**, pp. 173–183.
[10] Giel, P. W., Bunker, R. S., Van Fossen, G. J., and Boyle, R. J., 2000, "Heat Transfer Measurements and Predictions on a Power Generation Gas Turbine Blade," ASME Paper No. 2000-GT-209.
[11] Boyle, R. J., Luci, B. L., Verhoff, V. G., Camperchioli, W. P., and La, H., 1998, "Aerodynamics of a Transitioning Turbine Stator Over a Range of Reynolds Numbers," ASME Paper No. 98-GT-285.
[12] Ames, F. E., and Plesniak, M. W., 1997, "The Influence of Large-Scale, High Intensity Turbulence on Vane Aerodynamics Losses, Wake Growth, and the

Downloaded 28 May 2010 to 128.113.26.88. Redistribution subject to ASME license or copyright; see http://www.asme.org/terms/Terms_Use.cfm

Exit Turbulence Parameters," ASME J. Turbomach., **119**, pp. 182–192.
[13] Jouini, D. B. M., Sjolander, S. A., and Moustapha, S. H., 2001, "Aerodynamic Performance of a Transonic Turbine Cascade at Off-Design Conditions," ASME J. Turbomach., **123**, pp. 510–518.
[14] Radomsky, R. W., and Thole, K. A., 2002, "Detailed Boundary Layer Measurements on a Turbine Stator Vane at Elevated Freestream Turbulence Levels," ASME J. Turbomach., **124**, pp. 107–118.
[15] Boyle, R. J., Lucci, B. L., and Senyitko, R. G., 2002, "Aerodynamics Performance and Turbulence Measurements in a Turbine Vane Cascade," ASME Paper No. GT2002-30434.
[16] Zhang, Q., Lee, S. W., and Ligrani, P. M., 2004, "Effects of Surface Roughness and Turbulence Intensity on the Aerodynamic Losses Produced by the Suction Surface of a Simulated Turbine Airfoil," ASME J. Fluids Eng., **126**, pp. 257–265.
[17] Zhang, Q., and Ligrani, P. M., 2004, "Mach Number/Surface Roughness Effects on Symmetric Transonic Turbine Airfoil Aerodynamic Losses," J. Propul. Power, **20**(6), pp. 1117–1125.
[18] Christopher, R. J., Xavier, A. M., Friedrich, O. S., Charles, D. M., and Matthew, M., 1998, "High Pressure Turbine Vane Annular Cascade Heat Flux and Aerodynamic Measurements With Comparisons to Predictions," ASME Paper No. 98-GT-430.
[19] Coton, T., Arts, T., and Lefebvre, M., 2001, "Effects of Reynolds and Mach Numbers on the Profile Losses of a Conventional Low-Pressure Turbine Rotor Cascade With an Increasing Pitch-Chord Ratio," Proc. Inst. Mech. Eng., Part A, **215**(6), pp. 763–772.
[20] Chappell, J., Ligrani, P. M., Sreekanth, S., and Lucas, T., 2008, "Suction-Side Gill-Region Film Cooling: Effects of Hole Shape and Orientation on Adiabatic Effectiveness and Heat Transfer Coefficient," ASME Paper No. GT2008-50798.
[21] Jackson, D. J., Lee, K. L., Ligrani, P. M., and Johnson, P. D., 2000, "Transonic Aerodynamics Losses Due to Turbine Airfoil, Suction Surface Film Cooling," ASME J. Turbomach., **122**, pp. 317–326.
[22] Furukawa, T., and Ligrani, P. M., 2002, "Transonic Film Cooling Effectiveness From Shaped Holes on a Simulated Turbine Airfoil," J. Thermophys. Heat Transfer, **16**, pp. 228–237.
[23] Zhang, Q., Sandberg, D., and Ligrani, P., 2005, "Influence of Mach Number and Freestream Turbulence Intensity on the Aerodynamic Losses of a Turbine Vane," J. Propul. Power, **21**(6), pp. 988–996.
[24] Kline, S. J., and McClintock, F. A., 1953, "Describing Uncertainties in Single Sample Experiments," Mech. Eng. (Am. Soc. Mech. Eng.), **75**, pp. 3–8.
[25] Moffat, R. J., 1988, "Describing the Uncertainties in Experimental Results," Exp. Therm. Fluid Sci., **1**, pp. 3–17.
[26] Bammert, K., and Sandstede, H., 1980, "Measurements of the Boundary layer Development Along a Turbine Blade With Rough Surfaces," ASME J. Eng. Power, **102**, pp. 978–983.
[27] Denton, J. D., 1993, "Loss Mechanisms in Turbomachines," ASME J. Turbomach., **115**, pp. 621–656.
[28] Boyle, R. J., and Senyitko, R. G., 2003, "Measurements and Predictions of Surface Roughness Effects on Turbine Vane Aerodynamics," ASME Paper No. GT2003-38580.

Downloaded 28 May 2010 to 128.113.26.88. Redistribution subject to ASME license or copyright; see http://www.asme.org/terms/Terms_Use.cfm